Thermal Superinsulating Materials Made from Nanofibrillated Cellulose-Stabilized Pickering Emulsions

Clara Jimenez-Saelices, Bastien Seantier, Yves Grohens, Isabelle Capron

Thermal superinsulating materials made from nanofibrillated cellulose-stabilized Pickering emulsions

Clara Jiménez-Saelices, Bastien Seantier†, Yves Grohens†, Isabelle Capron***

*UR1268 Biopolymères Interactions Assemblages, INRA, 44316 Nantes, France

†IRDL, UBS, FRE CNRS 3744, 56100 Lorient, France

KEYWORDS: nanofibrillated cellulose (NFC), nanoparticle, biopolymer, Pickering emulsion, freeze-drying, aerogel, thermal superinsulation

ABSTRACT

Thermal superinsulating properties of biobased-materials are investigated via the structuration of aerogels through a biphasic system. Highly stable Pickering emulsions are produced using TEMPO-oxidized cellulose nanofibrils (NFC) adsorbed at an oil/water interface. NFCs form an entangled system of clusters of droplets that lead to excellent mechanical properties. The emulsions produced are strong gels that are further used as template to form aerogels. The freeze-dried emulsions result in porous bioaerogels with extremely low densities varying from 0.012 to 0.030 g/cm3. We describe a hierarchical morphology with three levels of porosity: an alveolar organization of larger macropores due to ice crystals, spherical smaller macropores

induced by the emulsion template, and mesoporous domains localized at the pore walls level. The low-density bioaerogels have compression moduli as high as 1.5 MPa and show plastic deformation up to 60% strain before the structure collapse. NFC aerogels have thermal superinsulating properties, which means that they have a thermal conductivity below that of air in ambient conditions. The lowest thermal conductivity obtained is 0.018 W/(m.K). In the context of the development of sustainable materials, we demonstrate that NFC-stabilized Pickering emulsions are excellent templates to produce fully biobased, mechanically strong thermal superinsulating materials.

INTRODUCTION

Emulsions are mixtures of two immiscible liquids that require surface-active species to obtain stable interfaces. When the stabilizers are colloidal particles, the emulsions are referred to as Pickering emulsions.[1, 2] These types of emulsions are more stable than classical ones that are stabilized with surfactants because the solid particles are irreversibly anchored at the drop interface. This results in a solid armor that prevents coalescence by steric repulsion. Moreover, such particle-stabilized emulsions are attractive from an environmental point of view because they globally reduce the amount of interfacial active agents required. Particles reported in the literature that are capable of stabilizing emulsions are very diverse. They have various chemical surface functions, natural or synthetic origins and different geometries and shapes.[3-7] As a renewable material, cellulose has a high potential and is one of the main abundant, biodegradable and sustainable molecules found in nature. Moreover, it is a promising and valid option for replacing petroleum-based surfactants and polymers with renewable resources.[8, 9] The use of microcrystalline cellulose to stabilize oil-in-water emulsions was first demonstrated by Oza *et al*.[10] Since that publication, many examples of Pickering emulsions stabilized with various types

of nanocelluloses have been reported.[11] For example, nanofibrillated celluloses (NFC),[12, 13] cellulose nanocrystals (CNC),[14-17] and bacterial nanocellulose[18, 19] have all shown their potential to stabilize emulsions. Interest in Pickering emulsions has been growing in recent years, especially for health and cosmetic applications where the use of surfactants is undesirable, and the use of Pickering emulsions as templates or intermediaries for complex structured materials is even more innovative. This concept has recently been used for the preparation of ultrastable wet foams[20-23] and for the production of a wide range of low-density, porous materials.[24, 25]

Aerogels are highly porous materials with very low densities in which the solvent of a gel is replaced by gas, leading to very moderate shrinkage of the solid network. Bioaerogels are aerogels prepared from biomass. The focus of a great deal of attention in recent years, they are mainly polysaccharide-based. Because polysaccharides are biocompatible and biodegradable, such aerogels are relevant in biomedical (scaffolds) and pharmacological (controlled release) applications.[26-31] Moreover, since they are light-weight, they are suitable for use as materials for thermal insulation and packaging, which currently consist mainly of plastic foams made from polystyrene or polyurethane.[32]

Some aerogels have thermal superinsulating properties: their conductivity is lower than that of air in room conditions.[33] This extraordinary property is due to their specific structure. Their low density limits the heat conduction of the solid phase and the contribution of the gas phase is reduced by narrowing the pore size below the mean free path of gas molecules in the air (approximately 70 nm). Silica aerogels are the most effective thermal superinsulating materials. However, they are not widely used at this time because of their mechanical fragility and relatively high production cost.

Several polysaccharides have been used to make bioaerogels. Nevertheless, there are only a few publications that deal with nanofibrillated cellulose,[34, 35] pectin,[36] chitosan,[37] alginate[38] and starch[39] aerogels with thermal conductivities of around 0.016−0.020 W/(m·K). These low values refer to the aerogel morphology, which is controlled by processing conditions. In general, bioaerogels are prepared via a three-step process, including dissolution of a polysaccharide, solution gelation, followed by drying processes. Highly porous cellulose aerogels have already been prepared from regenerated cellulose[27, 40-42] or from native bacterial or nanofibrillated cellulose.[43-46] Native cellulose is of particular interest because it does not require polymer dissolution. In addition, the long and entangled cellulose nanofibrils dispersed in aqueous media form a skeleton that prevents collapse during the solvent extraction. In all cases, the drying step is crucial as it determines the material's morphology. Freeze-drying and drying in supercritical conditions are known to preserve the network structure. However, the morphology of the porous material obtained is very different. Freeze-drying is a process in which the solvent present in the pores of the three-dimensional network of the gel is first frozen and then dried by sublimation under vacuum.[47] This process leads to the formation of large pores and channels ranging from several microns to tens of microns due to the growth of ice crystals.[48, 49] In supercritical conditions, the liquid/gas surface tension is zero because there is no liquid/gas meniscus. Thus, supercritical drying better preserves fine network structure, leading to the formation of mesopores that can improve the thermal insulating properties of aerogels. However, the main disadvantage of this method is that a solvent exchange step is mandatory.

The goal of the present work is to develop a new process to prepare a porous bioaerogel with high mechanical and thermal superinsulating properties. For this purpose, NFC-stabilized Pickering emulsion is used as a template in order to obtain hierarchical aerogel morphology.

Emulsions were first prepared and characterized. These emulsions serve as precursors for the formation of alveolar aerogels after freeze-drying. We thus demonstrate that the control of the emulsion's architecture allows the preparation of aerogels with a specific morphology by a simple freeze-drying step. We performed a detailed analysis of the density, morphology, mechanical and thermal insulating properties of the bioaerogels, demonstrating that the present strategy is very promising for the production of mechanically strong thermal superinsulators.

EXPERIMENTAL SECTION

Materials

An aqueous suspension of NFC at 1 wt% produced by TEMPO-mediated oxidation of spruce wood pulp was purchased from the Swiss Federal Laboratories for Materials Science and Technology (EMPA, Dübendorf, Switzerland). Dextran (100000 g/mol) and hexadecane were acquired from Sigma-Aldrich.

Characterization of NFC and suspension preparation

The 1.12 mmol/g carboxylate content was measured by conductometric titration with an automated Metrohm 905 Titrando system and TIAMO software (Metrohm, Switzerland).

The NFC dimensions were determined by atomic force microscopy (AFM) with a multimode setup equipped with a Nanoscope III-a (Bruker Nano, Santa Barbara, CA, USA). The AFM was used in contact mode imaging. The cross-section and the length of the NFC were analyzed from 100 height pictures with ImageJ software, version 1.6.0. The height of the NFC was considered so as to estimate the cross-section in order to limit the tip convolution effect. The NFC cross-section and length distribution are shown in Figure S1. A NFC cross-section of 4 nm and a minimum length of 450 nm were measured.

Osmotic concentration was performed using dextran solutions at 100 g/L to concentrate the NFC dispersions. A dialysis membrane, Espectra/Por®, with a molecular cutoff of 12 to 14 kDa, was used. Final concentrations of NFC dispersions varied from 0.2 g/L to 30 g/L. NFCs in aqueous media produce translucent and viscous or gel dispersions depending on the concentration.

Emulsion preparation and characterization

Hexadecane and NFC aqueous suspension were sonicated for 3 min by intermittent pulses with a dipping titanium tip at amplitude 2 (4 W/mL applied power) to prepare oil-in-water (o/w) emulsions. All the emulsions were prepared using a 20/80 oil/aqueous phase volume ratio.

Horiba LA-960 particle size distribution analyzer (Kyoto, Japan) was used to measure the individual average droplet diameters. A refractive index of 1.43 and 1.33 was used for hexadecane and water, respectively. The calibration for water as a reference was taken before each measurement. The measurements were carried out in duplicated. The diameter was expressed as the surface mean diameter D(3,2) (Sauter's diameter).

Transmission optical microscopy was used to visualize the droplets. Emulsions were diluted in distilled water, then poured onto a slide and observed with a BX51 Olympus microscope.

Scanning electron microscopy (SEM) was used to visualize the interface of polymerized styrene-in-water emulsions. Hexadecane and styrene have similar surface tensions (27 mN m^{-1} and 32 mN m^{-1}, respectively) and the same average drop diameter. We therefore estimate that the visualized beads provide a good estimate of what occurs in the liquid state. Consequently, styrene–AIBN mixtures (ratio 100:1 w/w) were mixed with aqueous NFC dispersions and emulsions were made via sonication. The styrene-in-water emulsions were then polymerized at

65°C for 48 hours. The dried beads were metallized with gold and visualized with a JEOL 6400F instrument.

Aerogel preparation and characterization

Bioaerogels were prepared by freeze-drying. Pickering emulsions with NFC concentrations ranging from 10 to 30 g/L were poured into aluminum molds and placed in a deep-freezer at −80°C for 24 h. Drying was carried out for 48 h using a SRK-Systemtechnik GT2 – 90° freeze-dryer. During drying process, the condenser temperature was of −50°C and the vacuum was below 0.01 mbar.

The bulk density ρ_{bulk} of the aerogels was calculated by dividing their weight by their volume. The weight of aerogels was determined at 50% relative humidity with an analytical balance (Mettler Toledo XS) and their volume was measured with a digital caliper. Porosity was calculated using Equation 1,[36] where the skeletal density $\rho_{skeletal}$ is the density of cellulose: 1.6 g/cm^3.[50]

$$\varepsilon\ (\%) = (1 - (\rho_{bulk} / \rho_{skeletal})) \times 100 \quad (1)$$

A JEOL JSM 6460LV scanning electron microscope was used to visualize the structure of the bioaerogels. Aerogel cross-sections were prepared by fracture in liquid nitrogen and metallized with gold before visualization.

The specific surface area was measured by nitrogen adsorption-desorption using the BET theory.[51] The isotherms were obtained using a Micromeritics 3Flex apparatus. Before the experiments, a vacuum degassing of samples at ambient temperature for 15 h was carried out.

The mechanical properties were characterized by uniaxial compression experiments in a MTS SYNERGIE 100. A loading cell of 100 N was used to obtain a complete stress-strain curve for each sample. The tests were carried out until the deformation of sample exceeded 70% and

displacement rate was 1 mm/min. Three cylindrical samples per formulation were tested (length/diameter ratio = 3/2).

The hot strip technique was used to measure the thermal conductivity, λ, of the aerogels. This device has been used previously for thermal characterization of aerogels.[52, 53] The calibration of the equipment is given in Figure S2. The tests were performed at atmospheric pressure in a temperature- and humidity-controlled room (21–22°C and 50% relative humidity). Five samples per formulation were tested.

RESULTS AND DISCUSSION

Emulsion architecture

Hexadecane-in-water Pickering emulsions were successfully prepared by varying the NFC concentrations introduced from 0.2 to 30 g/L. Figure 1a shows various NFC stabilized emulsions. Since hexadecane has a density lower than water, the oil droplets tend to go up. However, despite this creaming process, no variation in the drop size was observed. Thus, all the emulsions showed remarkable stability since they remained unchanged for more than one year. Moreover, the emulsion volume increased regularly with the amount of NFC introduced. Above an NFC concentration of 2 g/L, the complete volume of emulsions was filled with droplets (Figure 1a).

The average drop diameter as a function of NFC concentration is represented in Figure 1b, and the transmission optical micrographs of some emulsions are shown in Figure 1c. At low concentrations, the amount of NFC is too small to efficiently cover the small droplets produced by sonication. Consequently, the droplets coalesce, creating fewer larger ones. Thus, below 0.7g/L, isolated drops with diameters of around 20 μm were obtained (Figure 1c). This limited

coalescence process, characterized by a sharp decrease in the drop diameter, has previously been reported for other Pickering emulsions.[19] At higher concentrations, aggregates of interconnected small droplets are observed (Figure 1c). This behavior was previously reported in emulsions stabilized by unmodified NFC[54] or C*ladophora* cellulose nanocrystals.[55] This is due to the considerable length of NFC compared to the drop diameter. In addition, the small section and the presence of less organized domains confer high global flexibility to NFC, thus inducing a gel-like network of droplets with diameters of around 1 μm, leading to higher emulsion volume (Figure 1a). That explains why, above 0.7 g/L, the average size increases slowly with the concentration until reaching a plateau (Figure 1b). In fact, the laser scattering particle size analyzer measures the size of the aggregate that increases with concentration, but not the individual drop size that actually decreases with concentration. For NFC concentrations higher than 4 g/L, the whole emulsion is a large entangled continuous network of droplets that cannot be measured by granulometry due to the large size of the aggregates. As a consequence, a plateau value is reached. However, similar clusters of droplets were observed by optical microscopy for these samples, even when prepared with up to 30 g/L.

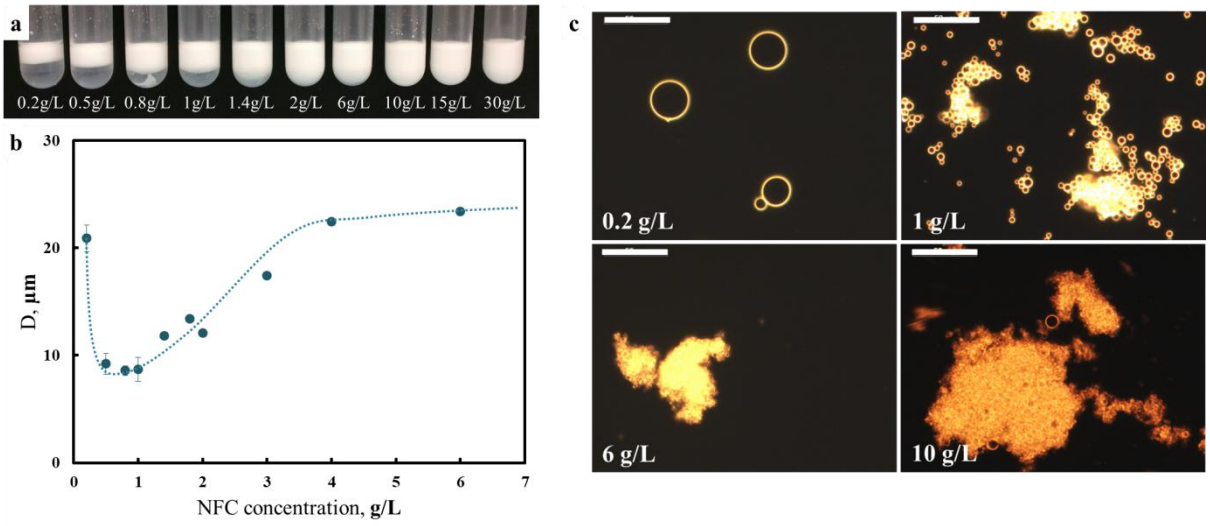

Figure 1. (a) Photographs of Pickering emulsions for increasing NFC concentrations in the water phase, ranging from 0.2 to 30 g/L. (b) Average diameters of droplets as a function of NFC concentration in the water phase for the hexadecane-in-water Pickering emulsions. The dashed line is a visual guide. (c) Transmission optical micrographs of hexadecane-in-water Pickering emulsions stabilized by NFC, with the corresponding concentrations given in the images. The scale bar is 50 µm.

The organization of NFC at the surface of the droplets was examined by scanning electron microscopy (SEM). SEM images of the polystyrene beads are shown in Figure 2, confirming that the entangled system of very small interconnected droplets was observed with a rather low coverage ratio of NFCs distributed at the surface of the droplets. The diameter of the droplets ranges from 100 nm to 1 µm. Such architecture with interconnected droplets in the submicron range has already been reported in a previous study[56] in which the viscoelastic properties of such emulsions were characterized. The values of the elastic modulus (G') of emulsions prepared at 6 g/L are higher than 500 Pa. This high modulus compared to dispersed NFCs was attributed to the

architecture of NFC-stabilized emulsions. The network of highly stable clusters of droplets strongly increased the mechanical properties of the emulsions. Thus, these emulsions seem to offer a perfect template for preparing highly porous material with a low pore size, an ultra-light density and good mechanical properties.

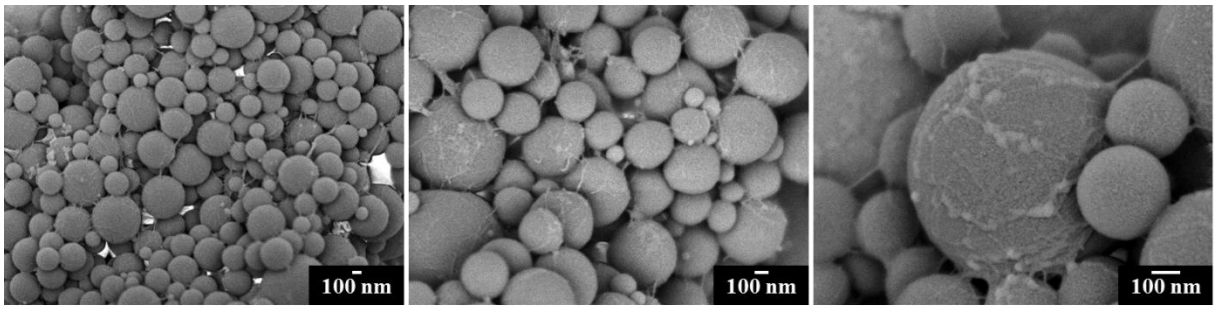

Figure 2. SEM images of droplets resulting from emulsions stabilized by NFC at 10 g/L.

Preparation of aerogels from emulsions

In order to obtain the whole emulsion under entangled aggregates of droplets with good mechanical properties and to avoid shrinkage during drying, Pickering emulsions with NFC concentrations ranging from 10 to 30 g/L were freeze-dried so as to form aerogels.

Monolithic and homogeneous aerogels were effectively obtained, as shown in Figure 3. Their densities vary from 0.012 to 0.030 g/cm^3 for NFC concentrations ranging from 10 to 30 g/L (Figure 3). As expected, the bulk density of the aerogels increases linearly with the NFC concentration. NFCs are naturally long and flexible and are entangled with each other. They form networks even at very low concentrations, making it possible to produce monolithic aerogels at lower concentrations than typical polysaccharide-based aerogels that involve a dissolution step.[43] Figure 3 compares bulk densities of the present aerogels prepared from emulsions with those of aerogels prepared from NFC hydrogels by conventional freeze-drying (CFD)[57] or by spray freeze-drying (SFD)[35] from earlier studies. CFD and SFD lead to aerogels

with extremely low densities. However, the emulsion templating method results in even lower densities. This is attributed to the presence of the droplets surrounded by NFC that includes air in the system, simultaneously preserving a stable and strong network that more effectively resists shrinkage during drying. The calculated porosity varied from 99% for aerogels prepared with 1 wt% NFC emulsion, to 98% for aerogels obtained from 3 wt% emulsion.

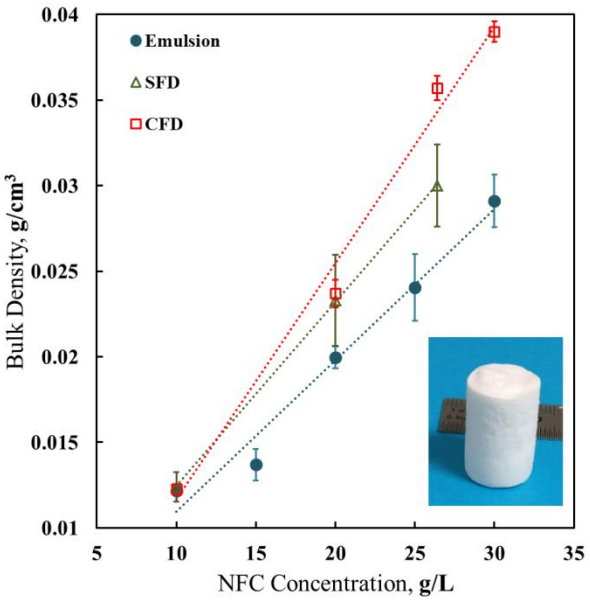

Figure 3. Comparison of bulk densities of NFC aerogels prepared by spray freeze-drying (SFD) or conventional freeze-drying (CFD) as a function of NFC concentration in suspension. The dashed line indicates a linear dependence of densities as a function of concentration. Data are taken from the present study and from the literature.[35, 57] Inset: Photo of a NFC aerogel.

Structural characteristics

Representative SEM images of aerogels prepared from Pickering emulsions stabilized by various concentrations of NFC are shown in Figure 4. Bioaerogels exhibited highly porous structures with an alveolar texture for all NFC concentrations. The cell size decreased with

increasing NFC concentration and aerogel density. The cell size decreased from 40 µm for the sample at 0.012 g/cm^3 to 5 µm for the sample at 0.030 g/cm^3. This specific morphology is a result of the drying process. The freeze-drying process consists of two steps: freezing and sublimation of the frozen liquids. The distribution of pore size, the pore shape and the connectivity of the porous network is the result of the shape of ice crystals that have been formed during freezing.[35] The emulsions are formed from two liquids: a continuous phase of water with a network of stable droplets of hexadecane that are interconnected by NFC. The crystallization temperature of hexadecane is 18°C. Thus, hexadecane crystallizes before water and the ice crystals grow between the frozen drops of hexadecane. As mentioned before, the increasing NFC concentration allows the stabilization of a larger number of smaller hexadecane droplets (Figure 4). This leads to the reduction of ice crystal size because of their confinement between the NFC network and the hexadecane droplets. Moreover, frozen hexadecane droplets may surround the ice crystals due to the fact that the growing ice crystals push the frozen hexadecane droplets to their edges. As a consequence, after sublimation, spherical porosity is visible in the walls of the alveolar cells (Figure 5). Furthermore, a second mechanism appears during the freezing process. Concentrated and confined at the interface, the NFCs undergo a lateral agglomeration upon freeze-drying, forming a 2D-sheet-like morphology. Attractive interactions such as hydrogen bonds and van der Waals forces hold the nanofibers together after the water is removed.[35]

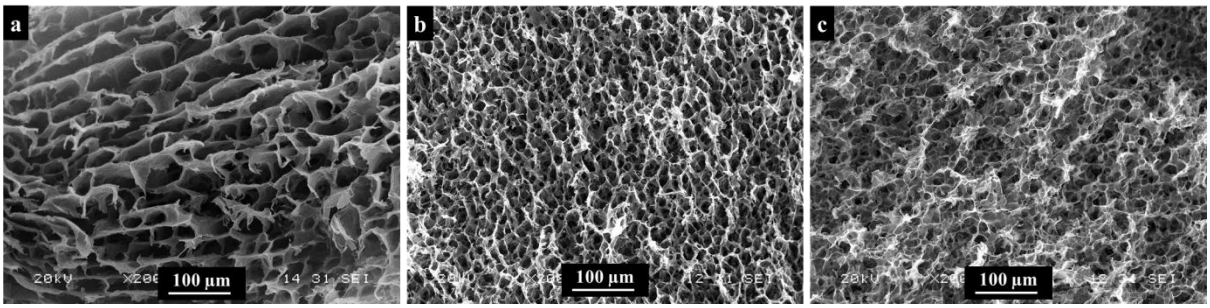

Figure 4. SEM images of bioaerogels prepared from NFC-stabilized emulsions at NFC concentrations of (a) 1, (b) 2 and (c) 3 wt%

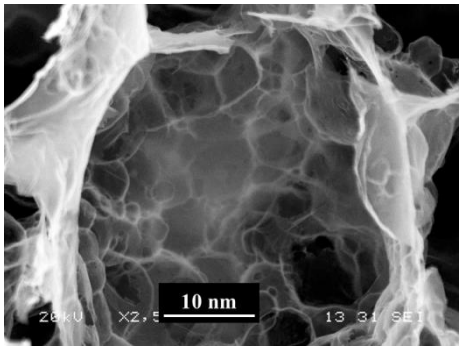

Figure 5. SEM images of bioaerogel prepared from 2 wt% NFC-stabilized emulsion showing two levels of porosity due to ice and emulsion droplets.

Nitrogen adsorption was used to determine the specific surface area and porosity characteristics of the NFC aerogels. This method has been widely used to study the microstructural characteristics of aerogels. However, it measures only a small fraction of the total pore volume.[34, 43] Since a full evaluation of the porosity was not possible with this technique, we used models to assess the presence of mesoporous domains. The isotherms show a gradual increase in the quantity of adsorbed nitrogen with pressure and a type A hysteresis loop during desorption (see Figure 6a for a typical isotherm). This is typical for mesoporous adsorbents with a strong adsorbate–adsorbent interaction. However, according to IUPAC classification,[58] the type IV isotherm is similar to the type II for low relative pressure, which is the case here. The isotherms therefore show the behavior of a hierarchical material with macropores, mesopores and micropores. The pore size of the aerogels estimated from the isotherms using the BJH approach[59] ranged from a few nanometers to 100 nm, with a most probable value around 30 nm. Macropores visible in SEM images are not measurable using the

BJH approach, confirming that, in addition to macropores visible by microscopy, the pore walls also have an internal mesoporosity, which explains the high porosity of aerogels.

The specific surface area S_{BET} was determined from the adsorption isotherms using BET analysis.[51] S_{BET} of the bioaerogels are between 65 and 13 m^2/g (Figure 6b). Higher densities corresponded to lower specific surface areas. The reason for this was that higher concentrations of NFC in the emulsion resulted in a higher degree of NFC aggregation. This is also in agreement with observations of the SEM micrographs in Figure 4. These values are significantly lower compared to those of regenerated cellulose aerogels (100-250 m^2/g)[26, 27] or native cellulose aerogels (500 m^2/g)[34] prepared by supercritical drying. The only reason for this difference is the drying method. Supercritical drying more effectively preserves the fine network structure formed.[60] The S_{BET} of such aerogels did not vary with the density, suggesting that the fibrils did not aggregate as the concentration increased. Consequently, aerogels prepared by supercritical drying have a fibrillar morphology with a specific surface area of several hundred m^2/g.[27, 40] In the case of freeze-drying, the ice crystal growth generate a pressure on pore walls that compresses the fibrils together, resulting in their aggregation. Yet, the prepared NFC bioaerogels have an extremely light-weight hierarchic architecture.

To conclude, the bioaerogels formed from Pickering emulsions exhibited highly porous structures with an alveolar texture and a closed porosity in the walls of the alveolar cells. The cell walls showed a 2D-sheet-like morphology with internal mesoporosity resulting from the NFC aggregation. The present values of specific surface area are consistent with a cellular foam structure and porous cell walls. It is similar to those obtained for bioaerogels made by freeze-drying.[43, 61] The complete microstructural characteristics of bioaerogels are shown in Figure S3.

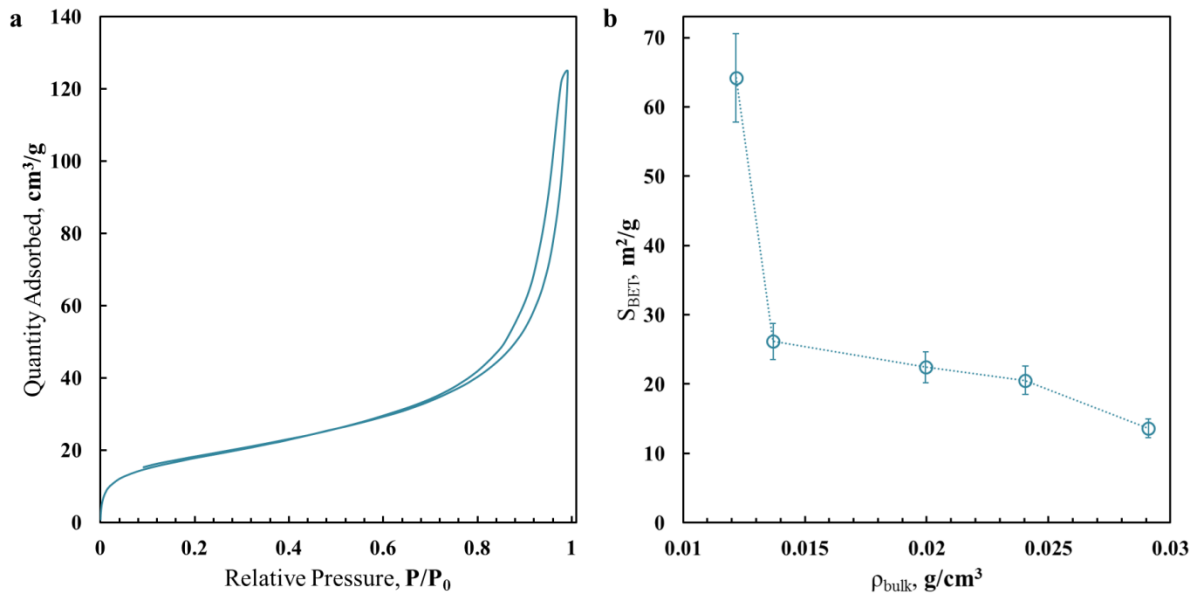

Figure 6. (a) Nitrogen adsorption–desorption isotherm of the aerogel. (b) Specific surface area of the aerogels estimated from the isotherms.

Mechanical properties

The mechanical properties of aerogels were studied by uniaxial compression. Figure 7a shows representative compression curves for the aerogels. The stress-strain curves show three defined regions. The first linear region results from the elastic and reversible deformation. Then, a gradual increase in the stress strain is observed that is attributable to a plastic deformation. Finally, a steep increase in the stress at strain > 50% is observed in the densification region where the opposing cell walls approach each other and eventually touch. The compressive modulus and the yield stress increase with the increase in bulk density.

The compressive behavior of foams and aerogels is commonly described by the Gibson and Ashby model[32] in which the compressive modulus follows the following power law as a function of density:

$$E \sim \rho^n \quad (2)$$

Honeycomb and open-cell foam have n ≈ 1 and n ≈ 2, respectively. However, in the case of aerogels, the exponent is higher, $2.5 < n < 4$ (n ≈ 3 for cellulose aerogels[62] and enzymatic NFC foams,[63] and n ≈ 3.7 for silica aerogels[64]).

Density controls the mechanical efficiency because it determines the network connectivity which is a key factor for the increase of the stiffness. In the open-cell foam model, the density changes by varying the thickness of the solid network but the network connectivity in not altered over the whole density range. This open-cell foam model (n ≈ 2) is not appropriate to explain aerogel behavior. It was shown that increasing density leads to the decrease of the pore size and specific surface (Figure 6b), which means that there is an increase of the NFC network thickness. However, increasing density also leads to increase network connectivity (Figure 4). The resistance to wall bending and collapse is thus increased, resulting in a higher compressive modulus and yield stress. Therefore, the heterogeneous network structures of aerogels result in a strong dependence of the modulus on the density. As a consequence, the present aerogels have an expected $n \approx 3$, which is similar to the one found for aerogels in the literature.

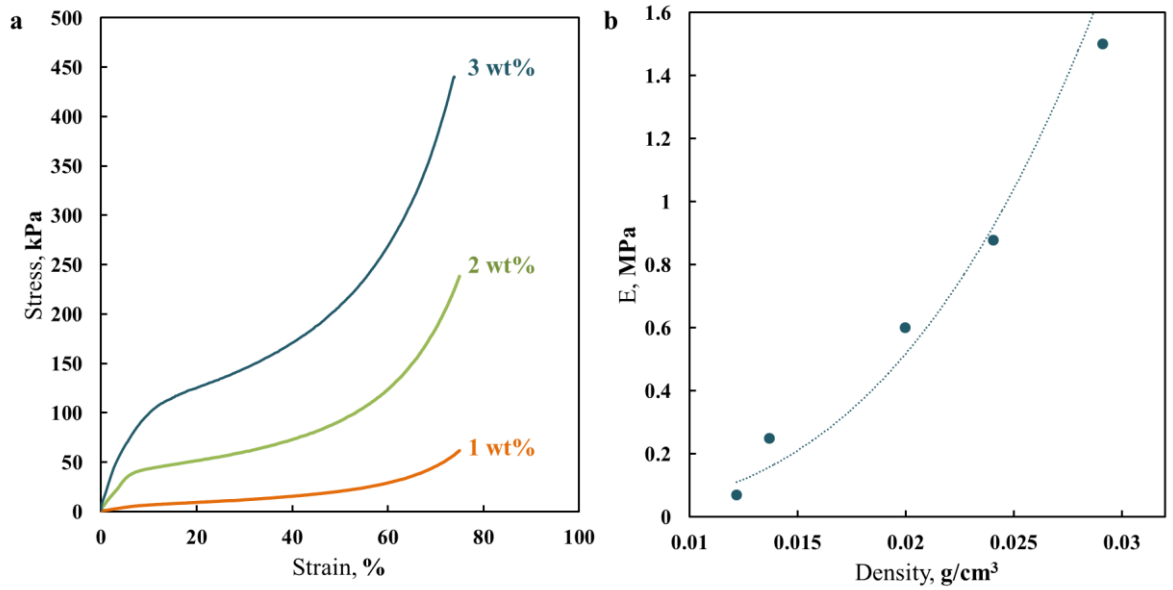

Figure 7. (a) Example of stress-strain uniaxial compression curves for bioaerogels prepared from 1, 2 and 3 wt% (b) Compressive modulus of the aerogels as a function of bulk density. The dashed line corresponds to power law approximation (n ≈ 3).

In Figure 8, moduli for the present NFC aerogels are compared to data collected from the literature for aerogels produced from native cellulose, regenerated cellulose, other polysaccharides and silica. It is interesting to note that aerogels prepared from native cellulose have a much lower density than the others. The present NFC aerogels showed compression moduli much higher than those of similar densities did. Moreover, according to the strong dependence of the compression modulus on the density (n = 3.2), it is expected that denser aerogels will have higher moduli than in the bibliography. Their enhanced mechanical properties may be due to their hierarchical structure that can be understood as a mixture between aerogel and foam. The wall cells showed the erratic and heterogeneous network of structures typical of aerogels prepared by supercritical drying. However, the alveolar texture was consistent with a cellular foam structure, as demonstrated by the values of specific surface area.

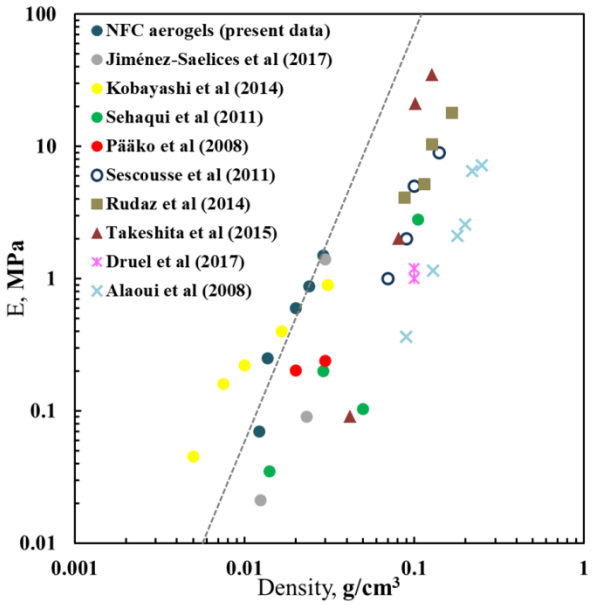

Figure 8. Comparison of compression moduli as a function of density for aerogels prepared from native cellulose (dark circles), regenerated cellulose (open circles), pectin (dark squares), chitosan (dark triangles), starch (asterisk) and silica (x symbols). Data are taken from the present study and from the literature.[34-37, 43, 62, 65, 66] The dashed line corresponds to the power law approximation ($n = 3.2$).

Thermal insulating properties

The heat transfer through porous materials can be described by three factors: the conduction in solid phase, λ_{solid}; the conduction through gas phase, λ_{gas}; and the radiative heat transfer through the pores, λ_{rad}. The total equivalent thermal conductivity, λ_{tot}, of porous materials can be calculated by a parallel flux model as the additive sum of these three contributions:[67]

$$\lambda_{tot} = \lambda_{solid} + \lambda_{gas} + \lambda_{rad} \quad (3)$$

The total thermal conductivity of aerogels was measured using the hot strip technique.[52, 53]

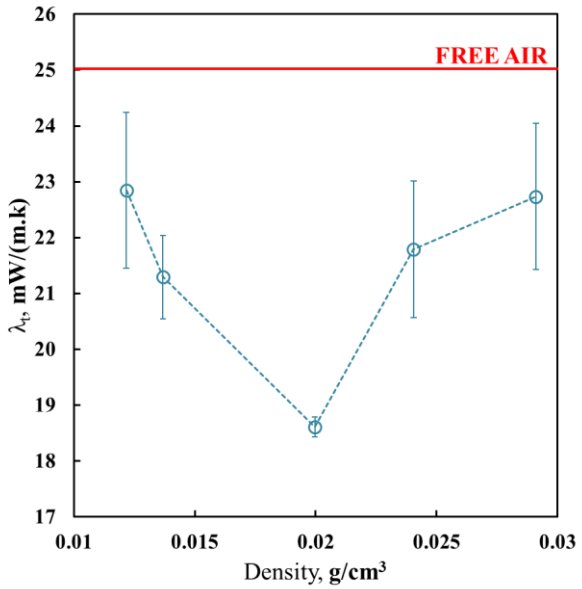

Figure 9. Thermal conductivity of bioaerogels as a function of bulk density. The dashed line is a visual guide. Air thermal conductivity is represented by a solid red line at 0.025 W/(m K).

Thermal conductivity values, λ_{tot}, of the bioaerogels are given as a function of bulk density in Figure 9. λ_{tot} decreases with density down to a minimum and then increases. This behavior, already reported in the literature, is typical of light-weight insulation materials.[34] The influence of solid conduction and radiation on the total equivalent thermal conductivity in porous materials strongly depends on the density.

At higher densities, the contribution of solid conduction, λ_{solid}, sharply increases, while that of radiative heat transfer, λ_{rad}, is reduced, inducing an optimum point where the sum of the contributions from radiation and solid conduction is at a minimum. On the other hand, the thermal conductivity of air (0.025 W/m.K) is independent of density and can be reduced by tuning the pore size.

The current aerogels prepared from Pickering emulsions have a thermal conductivity that varies between 0.018 and 0.023 W/(m·K). The mesoporous domains of ultra-porous aerogels favor the Knudsen effect because the air molecules can remain confined inside the pores that are smaller than their mean free path. As a result, λ_{gas} decreases. λ_{solid} was significantly reduced because of the ultra-low density of the aerogels. In addition, the close porosity also makes the radiative heat transfer, λ_{rad}, difficult within the structure because aerogels become more optically opaque, thereby minimizing this contribution. Consequently, all the aerogels have superinsulating properties, which means that their thermal conductivity is lower than that of air (0.025 W/(m·K)). The lowest thermal conductivity obtained was 0.018 W/(m·K).

Figure 10 compares the thermal conductivity prepared in this study with other thermal insulating polysaccharides and silica aerogels found in the literature as a function of density. Aerogels prepared from polysaccharides have thermal conductivities lower than commercial thermal insulators as mineral wools (0.033 W/(m·K)) and polystyrene foams (0.030 W/(m·K)).[68]

The thermal properties of the aerogels prepared in this study are comparable to those of silica aerogels, but they form a new generation of biomass-based thermal insulators.

These high performance properties highly depend on morphology. Consequently, the fine-tuning of the aerogel structure becomes a key stage in the preparation of insulation materials. The influence of the drying method on the morphology and properties of final porous materials has been widely studied and it has been demonstrated that supercritical drying preserves the inner porosity, whereas the growth of ice crystals during freezing leads to compact pore walls and large pores. It is for this reason that only aerogels prepared by supercritical drying have thermal superinsulating properties. However, as the results of the present study demonstrate, the use of an emulsion as a template for the preparation of porous materials constitutes a relevant approach for the control of the aerogel structure dried by conventional freeze-drying. As a result of this preparation process, the obtained aerogels combine similar or more effective thermal insulating properties with improved mechanical toughness.

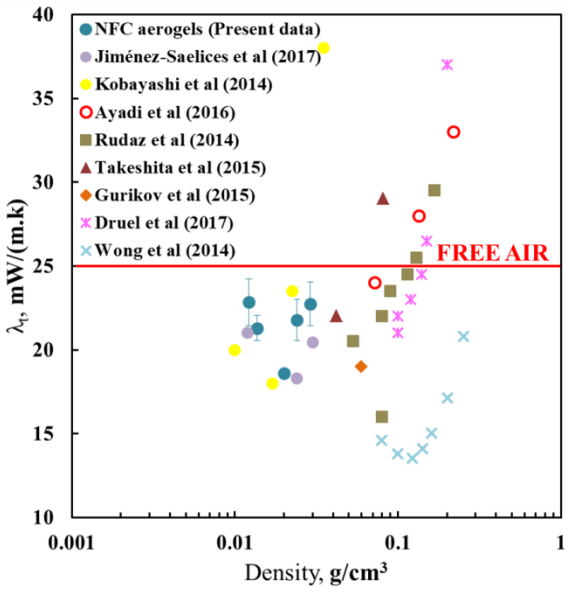

Figure 10. Comparison of thermal conductivity as a function of density for aerogels prepared from native cellulose (dark circles), regenerated cellulose (open circles), pectin (dark squares),

chitosan (dark triangles), alginate (dark rhombus), starch (asterisks) and silica (x symbols). Data are taken from the present study and from the literature.[34-3934-39, 69, 70]

CONCLUSIONS

NFC aerogels were successfully templated from Pickering emulsions. NFCs produced individual droplets at low concentrations and tended to form clusters of droplets at higher concentrations. These emulsions resulted in strong gels and served as precursors for the formation of aerogels by freeze-drying. The sublimation of such biphasic system is made possible due to the extreme resistance of the Pickering emulsions template that avoids shrinkage of the structure. The resulting NFC bioaerogels have an extremely light-weight hierarchical architecture. They exhibited highly porous structures with an alveolar texture and a closed porosity in the walls of the alveolar cells. The cell walls showed a 2D-sheet-like morphology with internal mesoporosity that resulted from the NFC aggregation. The bioaerogels exhibit a very low thermal conductivity of 0.018 W/(m·K), which is lower than that of stationary air. Such alveolar aerogels result in higher mechanical toughness than conventional silica aerogels. This strategy combines several levels of architectures, from a three-dimensional (3D) interconnected porous structure on the macroscale, down to a configuration of the walls at the nanoscale. It will definitely open a new route to the design of interesting biosourced alternatives such as superinsulating aerogels.

ASSOCIATED CONTENT

Figure S 1. NFC cross-section and length distribution. Figure S 2. Calibration of hot strip device. Figure S 3. Microstructural characteristics of bioaerogels. This material is available free of charge via the Internet at http://pubs.acs.org.

AUTHOR INFORMATION

Corresponding Author

*E-mail: Isabelle.capron@inra.fr

ACKNOWLEDGMENTS

We gratefully acknowledge Joëlle Davy (INRA, 44316 Nantes, France) and Anthony Magueresse (IRDL, UBS, Lorient, France) for their excellent technical assistance for SEM visualizations, as well as Nicolas Stephant (Institut des Matériaux Jean Rouxel, Université de Nantes) for access to the SEM equipment. We are equally grateful to Jean-Eude Maigret (INRA, 44316 Nantes, France) for his support in mechanical characterization, and to Bernard Cathala (INRA, 44316 Nantes, France) for his helpful discussions.

REFERENCES

1. Ramsden, W., Separation of Solids in the Surface-Layers of Solutions and'Suspensions'(Observations on Surface-Membranes, Bubbles, Emulsions, and Mechanical Coagulation).–Preliminary Account. *Proceedings of the royal Society of London* **1903,** *72*, 156-164.
2. Pickering, S. U., Emulsions. *Journal of the Chemical Society, Transactions* **1907,** *91*, 2001-2021.
3. Hsu, W. P.; Zhong, Q.; Matijević, E., The Formation of Uniform Colloidal Particles of Magnesium Fluoride and Sodium Magnesium Fluoride. *Journal of Colloid and Interface Science* **1996,** *181*, (1), 142-148.
4. Sugimoto, T.; Wang, Y., Mechanism of the Shape and Structure Control of Monodispersed α-Fe2O3Particles by Sulfate Ions. *Journal of Colloid and Interface Science* **1998,** *207*, (1), 137-149.
5. Binks, B. P.; Clint, J. H.; Mackenzie, G.; Simcock, C.; Whitby, C. P., Naturally Occurring Spore Particles at Planar Fluid Interfaces and in Emulsions. *Langmuir* **2005,** *21*, (18), 8161-8167.
6. Brandy, M.-L.; Cayre, O. J.; Fakhrullin, R. F.; Velev, O. D.; Paunov, V. N., Directed assembly of yeast cells into living yeastosomes by microbubble templating. *Soft Matter* **2010,** *6*, (15), 3494-3498.
7. Schmitt, V.; Destribats, M.; Backov, R., Colloidal particles as liquid dispersion stabilizer: Pickering emulsions and materials thereof. *Comptes Rendus Physique* **2014,** *15*, (8-9), 761-774.

8. Fratzl, P.; Weinkamer, R., Nature's hierarchical materials. *Progress in Materials Science* **2007,** *52*, (8), 1263-1334.
9. Klemm, D.; Heublein, B.; Fink, H.-P.; Bohn, A., Cellulose: fascinating biopolymer and sustainable raw material. *Angewandte Chemie International Edition* **2005,** *44*, (22), 3358-3393.
10. Oza, K. P.; Frank, S. G., Microcrystalline cellulose stabilized emulsions. *JOURNAL OF DISPERSION SCIENCE ANDTECHNOLOGY* **1986,** *7*, (5), 543-561.
11. Capron, I.; Rojas, O. J.; Bordes, R., Behavior of nanocelluloses at interfaces. *Current Opinion in Colloid & Interface Science* **2017,** *29*, 83-95.
12. Gestranius, M.; Stenius, P.; Kontturi, E.; Sjoblom, J.; Tammelin, T., Phase behaviour and droplet size of oil-in-water Pickering emulsions stabilised with plant-derived nanocellulosic materials. *Colloids and Surfaces a-Physicochemical and Engineering Aspects* **2017,** *519*, 60-70.
13. Winuprasith, T.; Suphantharika, M., Properties and stability of oil-in-water emulsions stabilized by microfibrillated cellulose from mangosteen rind. *Food Hydrocolloids* **2015,** *43*, 690-699.
14. Kalashnikova, I.; Bizot, H.; Bertoncini, P.; Cathala, B.; Capron, I., Cellulosic nanorods of various aspect ratios for oil in water Pickering emulsions *soft matter* **2013,** *9*, 952-959.
15. Kalashnikova, I.; Bizot, H.; Cathala, B.; Capron, I., Modulation of Cellulose Nanocrystals Amphiphilic Properties to Stabilize Oil/Water Interface. *Biomacromolecules* **2012,** *13*, (1), 267-275.
16. Aben, S.; Holtze, C.; Tadros, T.; Schurtenberger, P., Rheological Investigations on the Creaming of Depletion-Flocculated Emulsions. *Langmuir* **2012,** *28*, (21), 7967-7975.
17. Cherhal, F.; Cousin, F.; Capron, I., Structural Description of the Interface of Pickering Emulsions Stabilized by Cellulose Nanocrystals. *Biomacromolecules* **2016,** *17*, (2), 496-502.
18. Ougiya, H.; Watanabe, K.; Morinaga, Y.; Yoshinaga, F., Emulsion-stabilizing effect of bacterial cellulose. *Bioscience Biotechnology and Biochemistry* **1997,** *61*, (9), 1541-1545.
19. Kalashnikova, I.; Bizot, H.; Cathala, B.; Capron, I., New Pickering Emulsions Stabilized by Bacterial Cellulose Nanocrystals. *Langmuir* **2011,** *27*, (12), 7471-7479.
20. Du, Z.; Bilbao-Montoya, M. P.; Binks, B. P.; Dickinson, E.; Ettelaie, R.; Murray, B. S., Outstanding stability of particle-stabilized bubbles. *Langmuir* **2003,** *19*, (8), 3106-3108.
21. Dickinson, E.; Ettelaie, R.; Kostakis, T.; Murray, B. S., Factors controlling the formation and stability of air bubbles stabilized by partially hydrophobic silica nanoparticles. *Langmuir* **2004,** *20*, (20), 8517-8525.
22. Gonzenbach, U. T.; Studart, A. R.; Tervoort, E.; Gauckler, L. J., Ultrastable Particle-Stabilized Foams. *Angewandte Chemie International Edition* **2006,** *45*, (21), 3526-3530.
23. Stocco, A.; Rio, E.; Binks, B. P.; Langevin, D., Aqueous foams stabilized solely by particles. *Soft Matter* **2011,** *7*, (4), 1260-1267.
24. Binks, B. P., Macroporous silica from solid-stabilized emulsion templates. *Advanced Materials* **2002,** *14*, (24), 1824-1827.
25. Studart, A. R.; Gonzenbach, U. T.; Akartuna, I.; Tervoort, E.; Gauckler, L. J., Materials from foams and emulsions stabilized by colloidal particles. *Journal of Materials Chemistry* **2007,** *17*, (31), 3283-3289.

26. Fischer, F.; Rigacci, A.; Pirard, R.; Berthon-Fabry, S.; Achard, P., Cellulose-based aerogels. *Polymer* **2006,** *47*, (22), 7636-7645.
27. Gavillon, R.; Budtova, T., Aerocellulose: New Highly Porous Cellulose Prepared from Cellulose−NaOH Aqueous Solutions. *Biomacromolecules* **2008,** *9*, (1), 269-277.
28. Quignard, F.; Valentin, R.; Di Renzo, F., Aerogel materials from marine polysaccharides. *New journal of chemistry* **2008,** *32*, (8), 1300-1310.
29. Mehling, T.; Smirnova, I.; Guenther, U.; Neubert, R. H. H., Polysaccharide-based aerogels as drug carriers. *Journal of Non-Crystalline Solids* **2009,** *355*, (50), 2472-2479.
30. Alnaief, M.; Alzaitoun, M. A.; García-González, C. A.; Smirnova, I., Preparation of biodegradable nanoporous microspherical aerogel based on alginate. *Carbohydrate Polymers* **2011,** *84*, (3), 1011-1018.
31. García-González, C. A.; Alnaief, M.; Smirnova, I., Polysaccharide-based aerogels—Promising biodegradable carriers for drug delivery systems. *Carbohydrate Polymers* **2011,** *86*, (4), 1425-1438.
32. Gibson, L. J.; Ashby, M. E., *Cellular Solids. Structure and Properties*. 2nd ed.; Cambridge Solid Press: 1999.
33. Koebel, M.; Rigacci, A.; Achard, P., Aerogel-based thermal superinsulation: an overview. *J Sol-Gel Sci Technol* **2012,** *63*, (3), 315-339.
34. Kobayashi, Y.; Saito, T.; Isogai, A., Aerogels with 3D Ordered Nanofiber Skeletons of Liquid-Crystalline Nanocellulose Derivatives as Tough and Transparent Insulators. *Angewandte Chemie International Edition* **2014,** *53*, (39), 10394-10397.
35. Jiménez-Saelices, C.; Seantier, B.; Cathala, B.; Grohens, Y., Spray freeze-dried nanofibrillated cellulose aerogels with thermal superinsulating properties. *Carbohydrate Polymers* **2017,** *157*, 105-113.
36. Rudaz, C.; Courson, R.; Bonnet, L.; Calas-Etienne, S.; Sallée, H.; Budtova, T., Aeropectin: Fully Biomass-Based Mechanically Strong and Thermal Superinsulating Aerogel. *Biomacromolecules* **2014,** *15*, (6), 2188-2195.
37. Takeshita, S.; Yoda, S., Chitosan aerogels: transparent, flexible thermal insulators. *Chemistry of Materials* **2015,** *27*, (22), 7569-7572.
38. Gurikov, P.; Raman, S. P.; Weinrich, D.; Fricke, M.; Smirnova, I., A novel approach to alginate aerogels: carbon dioxide induced gelation. *RSC Adv.* **2015,** *5*, (11), 7812-7818.
39. Druel, L.; Bardl, R.; Vorwerg, W.; Budtova, T., Starch Aerogels: A Member of the Family of Thermal Superinsulating Materials. *Biomacromolecules* **2017,** *18*, (12), 4232-4239.
40. Hoepfner, S.; Ratke, L.; Milow, B., Synthesis and characterisation of nanofibrillar cellulose aerogels. *Cellulose* **2008,** *15*, (1), 121-129.
41. Liebner, F.; Haimer, E.; Potthast, A.; Loidl, D.; Tschegg, S.; Neouze, M.-A.; Wendland, M.; Rosenau, T., Cellulosic aerogels as ultra-lightweight materials. Part 2: Synthesis and properties 2nd ICC 2007, Tokyo, Japan, October 25–29, 2007. *Holzforschung* **2009,** *63*, (1), 3-11.
42. Sescousse, R.; Smacchia, A.; Budtova, T., Influence of lignin on cellulose-NaOH-water mixtures properties and on Aerocellulose morphology. *Cellulose* **2010,** *17*, (6), 1137-1146.
43. Pääkkö, M.; Vapaavuori, J.; Silvennoinen, R.; Kosonen, H.; Ankerfors, M.; Lindström, T.; Berglund, L. A.; Ikkala, O., Long and entangled native cellulose I nanofibers

allow flexible aerogels and hierarchically porous templates for functionalities. *Soft Matter* **2008,** *4*, (12), 2492-2499.

44. Liebner, F.; Haimer, E.; Wendland, M.; Neouze, M.-A.; Schlufter, K.; Miethe, P.; Heinze, T.; Potthast, A.; Rosenau, T., Aerogels from Unaltered Bacterial Cellulose: Application of scCO2 Drying for the Preparation of Shaped, Ultra-Lightweight Cellulosic Aerogels. *Macromolecular bioscience* **2010,** *10*, (4), 349-352.

45. De France, K. J.; Hoare, T.; Cranston, E. D., Review of Hydrogels and Aerogels Containing Nanocellulose. *Chemistry of Materials* **2017,** *29*, (11), 4609-4631.

46. Lavoine, N.; Bergström, L., Nanocellulose-based foams and aerogels: processing, properties, and applications. *Journal of Materials Chemistry A* **2017,** *5*, (31), 16105-16117.

47. Pajonk, G. M.; Repellin-Lacroix, M.; Abouarnadasse, S.; Chaouki, J.; Klavana, D., Proceedings of the Fifth International Workshop on Glasses and Ceramics from Gels From sol-gel to aerogels and cryogels. *Journal of Non-Crystalline Solids* **1990,** *121*, (1), 66-67.

48. Sehaqui, H.; Salajková, M.; Zhou, Q.; Berglund, L. A., Mechanical performance tailoring of tough ultra-high porosity foams prepared from cellulose I nanofiber suspensions. *Soft Matter* **2010,** *6*, (8), 1824-1832.

49. Lee, J.; Deng, Y., The morphology and mechanical properties of layer structured cellulose microfibril foams from ice-templating methods. *Soft Matter* **2011,** *7*, (13), 6034-6040.

50. Ganster, J.; Fink, H. P., Physical constants of cellulose. In *Polymer Handbook*, John Wiley and Sons ed.; E.H. Immergut, E.A. Grulke: 1999.

51. Brunauer, S.; Emmett, P. H.; Teller, E., Adsorption of gases in multimolecular layers. *Journal of the American Chemical Society* **1938,** *60*, (2), 309-319.

52. Bendahou, D.; Bendahou, A.; Seantier, B.; Grohens, Y.; Kaddami, H., Nano-fibrillated cellulose-zeolites based new hybrid composites aerogels with super thermal insulating properties. *Industrial Crops and Products* **2015,** *65*, 374-382.

53. Gustafsson, S. E.; Karawacki, E.; Khan, M. N., Transient hot-strip method for simultaneously measuring thermal conductivity and thermal diffusivity of solids and fluids. *J. Phys. D: Appl. Phys.* **1979,** *12*, (9), 1411-1421.

54. Cunha, A. G.; Mougel, J.-B.; Cathala, B.; Berglund, L. A.; Capron, I., Preparation of Double Pickering Emulsions Stabilized by Chemically Tailored Nanocelluloses. *Langmuir* **2014,** *30*, (31), 9327-9335.

55. Kalashnikova, I.; Bizot, H.; Bertoncini, P.; Cathala, B.; Capron, I., Cellulosic nanorods of various aspect ratios for oil in water Pickering emulsions. *Soft Matter* **2012,** *9*, (3), 952-959.

56. Jimenez Saelices, C.; Capron, I., Design of Pickering Micro- and Nanoemulsions Based on the Structural Characteristics of Nanocelluloses. *Biomacromolecules* **2018,** *19*, (2), 460-469.

57. Jiménez-Saelices, C.; Seantier, B.; Cathala, B.; Grohens, Y., Effect of freeze-drying parameters on the microstructure and thermal insulating properties of nanofibrillated cellulose aerogels. *J Sol-Gel Sci Technol* **2017**, 1-11.

58. Rouquerol, J.; Avnir, D.; Fairbridge, C. W.; Everett, D. H.; Haynes, J. H.; Pernicone, N., Recommendations for the characterization of porous solids. *Pure and Applied Chemistry* **1994,** *10*, (66), 1739-1758.

59. Barret, E. P.; Joyner, L. G.; Halenda, P. P., The Determination of Pore Volume and Area Distributions in Porous Substances. Computations from Nitrogen Isotherms. *Journal of the American Chemical Society* **1951,** *73(1)*, 373-380.

60. Buchtová, N.; Budtova, T., Cellulose aero-, cryo- and xerogels: towards understanding of morphology control. *Cellulose* **2016,** *23*, (4), 2585-2595.
61. Aulin, C.; Netrval, J.; Wågberg, L.; Lindström, T., Aerogels from nanofibrillated cellulose with tunable oleophobicity. *Soft Matter* **2010,** *6*, (14), 3298-3305.
62. Sescousse, R.; Gavillon, R.; Budtova, T., Aerocellulose from cellulose–ionic liquid solutions: Preparation, properties and comparison with cellulose–NaOH and cellulose–NMMO routes. *Carbohydrate Polymers* **2011,** *83*, (4), 1766-1774.
63. Martoïa, F.; Cochereau, T.; Dumont, P. J. J.; Orgéas, L.; Terrien, M.; Belgacem, M. N., Cellulose nanofibril foams: Links between ice-templating conditions, microstructures and mechanical properties. *Materials & Design* **2016,** *104*, 376-391.
64. Woignier, T.; Phalippou, J., Mechanical strength of silica aerogels. *Journal of Non-Crystalline Solids* **1988,** *100*, (1-3), 404-408.
65. Alaoui, A. H.; Woignier, T.; Scherer, G. W.; Phalippou, J., Comparison between flexural and uniaxial compression tests to measure the elastic modulus of silica aerogel. *Journal of Non-Crystalline Solids* **2008,** *354*, (40–41), 4556-4561.
66. Sehaqui, H.; Zhou, Q.; Berglund, L. A., High-porosity aerogels of high specific surface area prepared from nanofibrillated cellulose (NFC). *Composites Science and Technology* **2011,** *71*, (13), 1593-1599.
67. Ebert, H.-P., Thermal Properties of Aerogels. In *Aerogels Handbook*, Aegerter, M. A.; Leventis, N.; Koebel, M. M., Eds. Springer New York: 2011; pp 537-564.
68. Al-Homoud, D. M. S., Performance characteristics and practical applications of common building thermal insulation materials. *Building and Environment* **2005,** *40*, (3), 353-366.
69. Wong, J. C. H.; Kaymak, H.; Brunner, S.; Koebel, M. M., Mechanical properties of monolithic silica aerogels made from polyethoxydisiloxanes. *Microporous and Mesoporous Materials* **2014,** *183*, 23-29.
70. Ayadi, F.; Martín-García, B.; Colombo, M.; Polovitsyn, A.; Scarpellini, A.; Ceseracciu, L.; Moreels, I.; Athanassiou, A., Mechanically flexible and optically transparent three-dimensional nanofibrous amorphous aerocellulose. *Carbohydrate polymers* **2016,** *149*, 217-223.

Table of Contents Graphic